Heat dissipation enhancement of an industrial totally-enclosed-fan-cooled motor through frame designs

Chia-Wei Kuo and Mei-Jiau Huang

Department of Mechanical Engineering, National Taiwan University, Taipei, Taiwan

ABSTRACT

New frame structures of an industrial totally-enclosed-fan-cooled (TEFC) motor were designed and numerically explored for the sake of heat dissipation enhancement. Several attempts were made in removing hot spots. First of all, the few large cooling ducts which are usually embedded within the frame for forming a closed internal flow are replaced by numerous small cooling ducts, uniformly distributed along the azimuthal direction. The walls between neighboring cooling ducts act like inner fins which help heat transfer from the interior of the motor to the outer surface of the frame; optimally spaced outer fins pass heat to the ambient air next. Secondly, a flat plate is added to cover the outer fins in the bottom of the motor for suppressing the flow leakage and therefore enhancing the heat dissipation there. Two new frames are so designed and simulations confirm that both successfully achieve the designing goals: a maximum frame temperature below 130°C and a maximum azimuthal temperature difference below 10°C.

Keywords: Totally-enclosed-fan-cooled motor; Heat dissipation; Frame design; Cooling duct

1. Introduction

A noticeable amount of heat is usually generated when an industrial motor is in operation. The high temperature deteriorates the motor efficiency and is unwanted. In general, the lifetime of the electrical insulation system for wires is halved for a temperature rise of 10°C. On the other hand, the performance is better when the stator windings are at about the same temperature. The electrical insulation system used in electric motors is divided into different classes by temperature and temperature rise [1]. As far as an industrial totally-enclosed-fan-cooled (TEFC) motor is concerned, an internal fan and an external fan are often employed to achieve heat dissipation purpose. Typically, the internal fan causes a circulating air flow inside the motor, responsible for cooling the rotor and stator; the flow pathway is closed through cooling ducts embedded in the frame, where air is cooled down by transferring heat to the frame. The external fan on the other hand causes a forced convection outside the frame; heat dissipation is enhanced by flat-plate fins mounted on the frame.

To further improve the heat dissipation, Telore et al. [2] recommended D-shaped cooling ducts because of its lower flow resistance compared with traditional rectangular cooling ducts. Lordo and Rudisch [3] mounted fins on both the outer and the inner walls of the frame and had them aligned so that heat can be conducted directly from the inner fins to the outer fins. Hashish [4] installed oblique tabs on the inner wall of the frame to increase flow randomness and the contact time/area between fluid and solid. The idea of using protrusions to assist heat transfer was also seen in the design of Evon and Martin [5] who mounted a plurality of fins to the stator inside the frame. Dawsey et al. [6] further enclosed such a stator by a cooling jacket. Kinoshita [7][8] improved the internal structure of the wind shield and inserted air deflectors at suitable locations to increase the flow pressure and decrease the noise. Beatty et al. [9] embedded pipes in the stator and connected them to metal sheets or cups at turns; a refrigerant flows inside the pipes to cool the stator. Smith et al. [10] constructed a cooling jacket consisting of axial channels in which a refrigerant flows.

In literature, staggered, perforated, and wavy fin arrays were proposed for heat transfer enhancement because they can increase temperature gradient near the fin surface or increasing flow randomness [11]. Leon et al. [12] confirmed the staggered fins have a stronger heat dissipation power although they have a smaller solid-fluid contact area than traditional in-line fins. Lee et al. [13] further proposed the oblique staggered fins for simultaneously suppressing boundary layer in additional to generating flow disturbances. For the perforated fin arrays, Shaeri et al. [14] stated that the larger the porosity, the higher the associated heat dissipation power is. Ismail et al. [15] argued that circular perforations result in better thermal and fluid dynamic performances than other types such as rectangular ones and triangular ones. For wavy fin arrays, higher heat dissipation was attributed to a wider flow channel for in-line layout by Islamoglu and Parmaksizoglu [16] and to a larger wavy angle for staggered layout by Naphon [17]. Other efforts in the fin geometry for heat transfer enhancement include increasing fin height in the streamwise direction [18], using reverse-trapezoidal fins [19], reducing the gap between the wind shied and fin tips [20], and so on. Soodphakdee et al. [21] investigated seven different types of fins, including parallel/staggered

flat-plate fins, in-line/staggered circular pins, in-line/staggered square pins, and staggered elliptic pins. They found under a fixed pressure drop, the staggered circular pins have a highest convection heat transfer coefficient but under a fixed pumping power, it is the staggered flat-plate fins perform best. However a better thermal performance is always accompanied with a larger flow resistance. A nice review of heat transfer enhancement in different types of extended surfaces can be found in Ganorkar and Kriplani [23].

Besides the fin geometry, an optimized fin spacing is also important. An optimized fin spacing usually corresponds to a minimum overall thermal resistance given a pool of design parameters, such as the fin height, the fin thickness, the width of the base-plate where fins are to be mounted, the pumping power, and/or the inlet velocity. Bar-Cohen and Rohsenow [24] considered natural convection and flat-plate fins. They first analyzed the relations between Nusselt number and the Rayleigh number for two limiting cases, zero and infinite fin spacing and then employed the asymptotic method proposed by Churchill and Usage [25] to determine the optimized fin spacing. Bejan and Sciubba [26] and Bejan and Morega [27] considered laminar and turbulent forced convection respectively. Empirical relations were employed first to evaluate the total heat transfer rates of the two limiting cases; they then determined the optimized spacing by equating the two rates. A recent application was executed by Canhoto and Reis [28] who aimed at a maximum heat transfer density. Knight et al. [29] investigated flat-plate fins with no bypass. An optimized fin spacing and fin thickness were targeted with the base-width and the fin height fixed. Hossain et al. [30] took the bypass effect into consideration. The minimum entropy theory was employed by Shih and Liu [31] for an optimized design.

In spite of fruitful results, most of the existing studies concentrate on applications in small-electronic devices, instead of large mechanical systems such as an industrial TEFC motor which is of interest in the present work. Some preliminary simulations done by the authors find that not many of these skills are useful for large mechanical systems with large Reynolds numbers. Flat plates are still the best choice, to the authors' knowledge, for an industrial TEFC motor. Besides, it is also noticed that a modification of fins only is not sufficient to maintain the whole motor at low enough and uniform enough temperature; hot spots are unavoidably caused by the cooling ducts. An overall modification of the motor frame becomes necessary. In this work, we aim at new inventions of the frame of an industrial TEFC motor which satisfies the B-class of the electrical insulation system, namely a maximum temperature of 130°C and a maximum azimuthal temperature difference below 10°C. However a whole simulation of the motor, including all the key components such as rotor, stator, fans, and so on, is extremely difficult and time-consuming. In this work, we also aim at developing a simplified numerical model that allows us performing the thermo-fluid analysis outside the motor frame without incorporating components inside. The invention of the new frame will take the influence of the cooling ducts, the optimization of fin spacing, and the floor effect into consideration.

The rest of this paper is arranged as follows. The proposed simplified motor model is

introduced in Sec.2 first; also presented is the simulation result of an existing industrial TEFC motor and its comparison with experimental measurement. The validity of the proposed model is so confirmed. In Sec.3, we propose two new frame inventions and verify their meeting the temperature criteria via simulation. Conclusion is given at last in Sec.4.

2. Numerical modelling

2.1 Problem description

A TEFC motor is basically composed of rotor, stator, wind shield, frame integrated with flat-plate fins, internal and external fans, and stands as illustrated in Figure 1. The rotor and stator (not shown in Figure 1) are placed inside the frame that is supported by the stands. The internal fan (not shown in Figure 1 either) generates an air flow passing through the rotor and stator; the heated air then flows into cooling ducts which are embedded in the frame and transfers heat to the frame before it gets back to the fan and forms a circulating flow. The external fan mounted outside the frame (and inside the wind shield) generates a forced convection to cool down the frame. Flat-plate fins on the frame help dissipating heat to the ambient air. Both internal and external fans are mounted on the motor shaft.

In the industrial TEFC motor shown in Figure 1, four cooling ducts are embedded in the motor frame. The rectangular duct labeled “4” is one of them; a second one is obscured by the stand 5. The remaining two locate on the other side of the motor. These rectangular ducts provide pathways for the internal flow. Although the internal flow helps cooling down the rotor and the stator by convection, it blocks heat transfer directly from the interior of the motor to the outer surface of the frame. Unacceptably high frame temperature may thus occur. The purpose of this research is to design a new frame structure in order to obtain a frame temperature below the maximum allowable one and as uniform as possible. To avoid the tremendously large computational amount of simulating a whole motor (including all key components and the coupling between the thermos-fluid flow field and the electromagnetic field), we propose below a simplified model that involves thermo-fluid analysis only and is good enough for investigating the heat dissipation power of a motor frame.

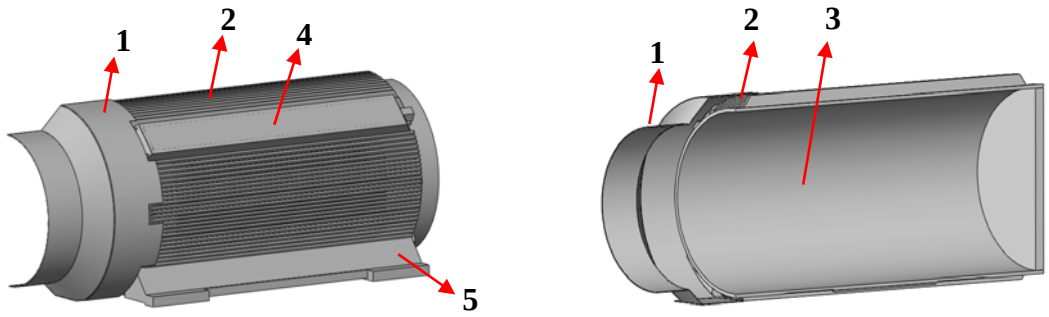

Figure 1. An external view and an internal view of a TEFC motor: in which the wind shield **1**, fins **2**, the inner surface of the frame **3**, a cooling duct **4**, and a stand **5** are marked.

2.2. Simplified motor model

A complete numerical model for the motor is extremely difficult. To make it tractable, simplification is necessary. Several efforts are thus attempted and explained below.

2.2.1. Numerical model

First of all, because we aim at a better frame for heat dissipation enhancement, we focus only on the external flow. That means neither the internal flow nor the electromagnetic field inside the motor is simulated; instead experimentally measured heat flux distribution over the inner surface of the frame is approximately imposed. For simplicity, the external fan is not simulated either. We simply assume that air at room temperature spurts from the gap between the wind shield and the frame at a pre-known velocity along the axial direction. As it passes the flat-plate fins on the outer surface of the frame, heat transfer occurs and the motor is cooled. Furthermore, because none of the components inside the motor is simulated, it is no way to solve the flow field inside the cooling ducts either. A characteristic temperature and a mean velocity are thus assumed for the flow inside the cooling ducts based on some experimental measurements. The energy conservation principle is employed to compute the heat transfer between the flow and the walls of a cooling duct, which will be explained in detail later.

Consequently, we end up with a numerical model which contains only the wind shield and the motor frame. Figure 2 shows such a motor standing on the ground within a sufficiently large computational domain. Due to the geometric symmetry with respect to the plane z=0, only a half motor needs building and simulating. Finally to examine the adequacy of the cooling power of a motor frame, we apply the B-class temperature criteria onto the inner surface of the frame. The temperature of components inside the motor must be even higher. A maximum allowable temperature less than 130°C might be employed for safety. On the other hand, as long as the temperature uniformity inside the motor is fine, the requirement of the temperature uniformity over the inner surface of the frame implies the frame structure is capable of maintaining the uniformity.

Figure 2. The computational domain: (a) the *x*-*y* view, (b) the *y*-*z* view, (c) an isometric view.

2.2.2. Boundary conditions

As mentioned above, a heat flux distribution is imposed at the inner surface of the frame. Experimental experiences show more heat is generated in the middle of the motor than near the two ends along the streamwise (x) direction. A uniform heat flux q_1 is thus imposed at the middle half surface (called midstream part hereafter) and q_2 in the remaining parts near the two ends (called the upstream and downstream parts hereafter). The inner surface of the vertical plate at the downstream side of the motor is assumed adiabatic (q=0) on the other hand. A uniform air flow at room temperature T_∞ and velocity U_∞ spurts from the annular opening between the wind shield and the outer surface of the frame. Because the wind shield locates in front of the annular opening, it is hardly thermally contaminated. It is therefore reasonable to assume a uniform temperature T_∞ on all the surfaces of the wind shield. Finally the temperature at all boundaries of the computational domain including the ground is assumed at room temperature T_∞ as well. A static pressure of 1atm is imposed at all these boundaries except the floor. No-slip boundary condition is imposed at all solid surfaces. Most of these thermal boundary conditions are illustrated in Figure 3.

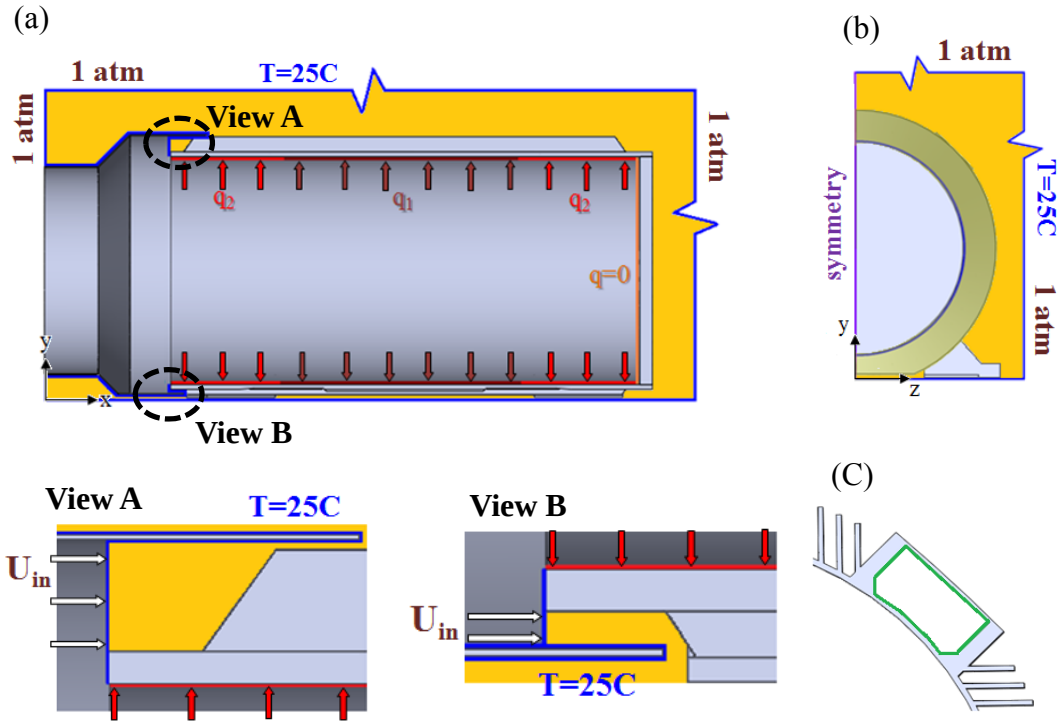

Figure 3. The boundary conditions: (a) the *x*-*y* view, (b) the *y*-*z* view, (c) an enlarged *y*-*z* view of a cooling duct.

As far as heat transfer between the solid part and the fluid part is concerned, it is solved mostly by imposing the continuity of temperature and heat flux at the interfaces. Because the flow inside the cooling ducts is not simulated, we need a model to capture its effect. The flow inside the cooling

ducts is usually cooler than the inner surface of the frame but hotter than the outer surface. Nonetheless, when steady, the net heat transfer rate between the flow and all the inner surfaces of the duct should be zero. For simplicity, we assume a characteristic temperature T_{in} and a characteristic velocity U_{in} for the flow and a mean convection heat transfer coefficient h_{in} between the flow and the inner surfaces of the duct. Consequently

$$\int_{A_{duct}} h_{in}\left(T_{in}-T_s\right)dA=0$$

or

$$T_{in}=\int_{A_{duct}} T_s dA \Big/ A_{duct} \tag{1}$$

where A_{duct} is the total contact area between the solid and the fluid and T_s is the temperature of the inner surface of the duct.

The convection heat transfer coefficient h_{in} is evaluated based on the empirical equation shown below [32]:

$$Nu_{D_h}\equiv\frac{h_{in}D_h}{k_{air}}=\frac{\left(f/2\right)Re_{D_h}Pr}{0.9+\left(g-7.65\right)\sqrt{\left(f/2\right)}} \tag{2}$$

$$g=4.8\cdot\left(k_s^+\right)^{0.2}Pr^{0.44} \tag{3}$$

$$k_s^+=\frac{k_s U_{in}}{\nu_{air}}\sqrt{f/8} \tag{4}$$

$$\frac{1}{\sqrt{4f}}=-2\,log_{10}\left[\frac{k_s}{3.7D_h}-\frac{5.02}{Re_{D_h}}log_{10}\left(\frac{k_s}{3.7D_h}+\frac{13}{Re_{D_h}}\right)\right] \tag{5}$$

where D_h is the hydraulic diameter of the cooling duct, k_{air} is the air thermal conductivity, f is friction coefficient, Re_{D_h} is the Reynolds number based on U_{in} and D_h, Pr is Prandtl number, k_s is surface roughness of the cast iron (0.26mm), and ν_{air} was the kinematic viscosity of air.

The commercial code ANSYS-FLUENT is employed to solve the thermal and flow fields of the system. The Navier-Stokes equations and the thermal energy equation are solved. The transient RANS RNG k-ε turbulence model is employed, in conjunction with a standard wall function, to capture the turbulent effects. The SIMPLE-C algorithm with 1st-order upwind scheme is selected to resolve the governing equations. The effects of radiation and natural convection are ignored. Steady simulation results are targeted. Equations (1)~(5) are implemented in the following way. The empirical value for U_{in} is given first; the Reynolds number Re_{D_h} can be calculated then. Based on calculated Re_{D_h} and the roughness k_s, the friction coefficient f and the convection heat transfer

coefficient h_{in} can be obtained by using Equations (2)~(5). The heat transfer rate between the inner surface of the duct and the air is estimated based on h_{in} and an initially guessed T_{in}; it becomes part of the thermal boundary conditions then for solving the thermal field including the surface temperature T_s. Equation (1) is now used to calculate the new T_{in} for the next time step. A convergence is expected when the system becomes steady.

2.3. Validation

Several tests were performed to ensure the validity of the proposed numerical method. First we examine the suitability of the RNG k-ε turbulence model by repeating the simulation of a flat-plate fin array with a zero angle of attack in Velayati and Yaghoubi [34]. The obtained Nusselt numbers at several Reynolds numbers ($>10^4$) which are often observed in the flow associated with the industrial TEFC motors are shown in Figure 4. As seen the present simulation results agree well with the experimental data measured by Velayati and Yaghoubi [34]; the agreement is poorer at lower Reynolds numbers because the grid resolution near the wall is designed high for high Reynold numbers. This test reveals both the employed mathematical models and the grid system are acceptable.

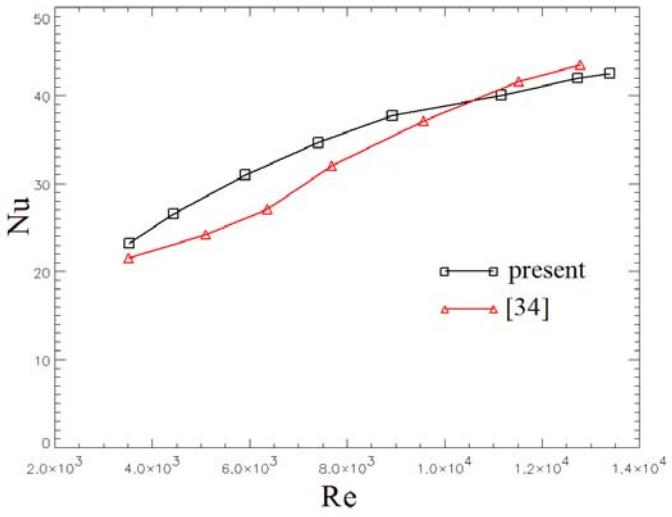

Figure 4. The Nusselt number versus Reynolds number for a flat-plate fin array.

We now try to simulate the model motor shown in Figure 2. The computational domain has a size of $3.88L \times 12.40R \times 11.28R$, where L is the length of the fins integrally formed on the outer surface of the frame and R is the inner radius of the frame. The domain size is determined by gradually enlarging the computational domain and repeating the simulation until no unphysical recirculation flow is observed in the far field. A hybrid 3D mesh consisting of structured and unstructured grids is employed. The former is mainly applied to the solid fins and the latter is used in the remaining solid parts and the fluid region. Furthermore, the computational domain is divided into three regions (see Figure 2); the grid resolution is gradually enhanced from far to near. Grid

points in the neighborhood of the ground were also carefully refined until reasonable flow pattern was obtained. A grid with a total of 9.41 million cells is finally employed after several grid tests.

A comparison with experimental measurements is made to examine the validity of the simulation method. Given the experimental conditions: T_∞=25°C, U_∞=14.4m/s ($\mathrm{Re}_\infty=U_\infty L/\nu_{air}\approx 1.5\times10^6$), U_{in}＝5m/s, and a total heat dissipation rate of 29kW, we choose q_1＝8658 W/m^2 and q_2＝5197W/m^2. The convection heat transfer coefficient (h_{in}) is found to be 30.8W/m^{2}K, evaluated by Eqns.(2)-(5). Flow patterns on two X-Y cross sections are shown in Figure 5; they both look reasonably well. The ambient air on the top is dragged downward first and toward the positive X direction (the streamwise direction) next by the air jet spurting from the gap between the wind shield and the motor frame and between the fins. Air injected into the spacing between neighboring fins gradually moves upward due to the growth of the boundary layer on the outer surface of the frame, resulting in a decreasing flow rate and consequently a decreasing heat dissipation rate with increasing downstream distance. The recirculation region behind the motor is caused by the sudden expansion.

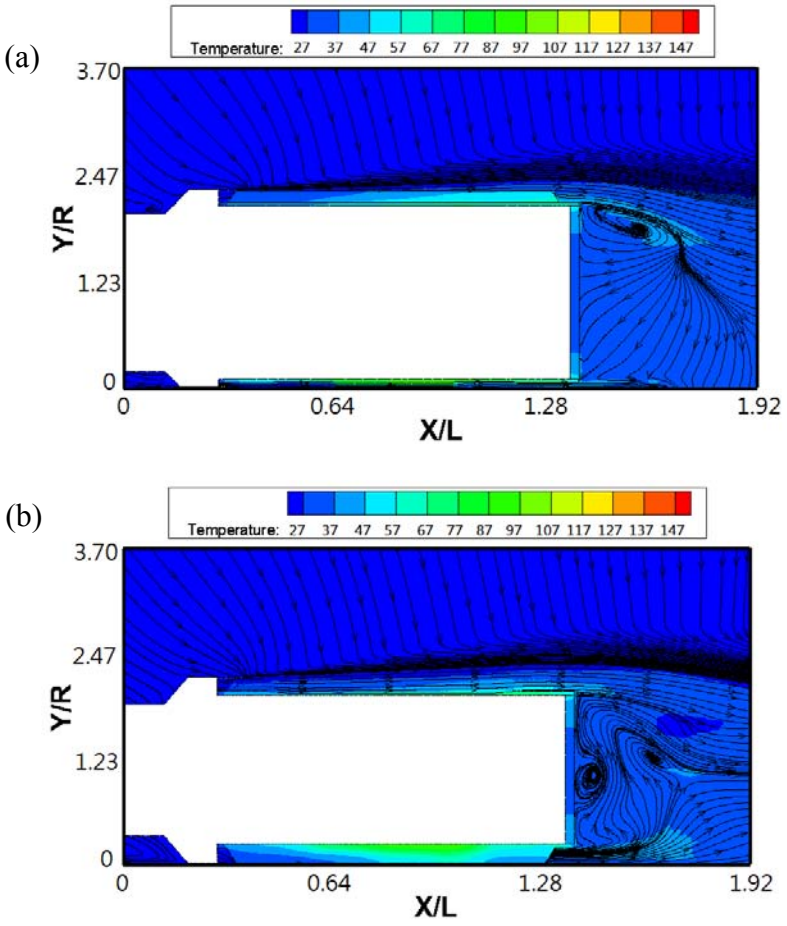

Figure 5. The flow patterns with temperature contours near the motor at (a) z＝0, (b) z＝0.49R.

Figure 6 shows the temperature distribution on a Y-Z cross section in the midstream region. The steady temperature of air in the cooling ducts is found to be 73°C. Obviously heat is transferred from the inner surface of the frame to the air and the side walls and successively transferred to the external flow. Also observed is heat seemingly accumulated in the bottom part of the frame.

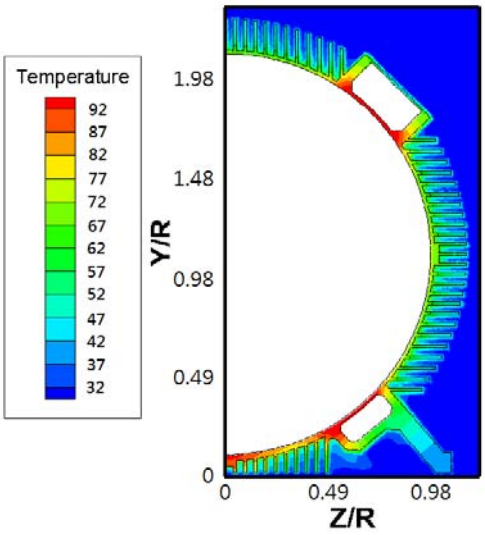

Figure 6. The temperature distribution on a Y-Z cross section in the midstream region (*x/L*=0.96).

For a further validation, a temperature snapshot of the motor in steady operation is shown in Figure 7, compared with the experimental measurement. The temperature distributions look similar, hotter near the downstream end and on the outer surface of the cooling ducts. The agreement is qualitatively acceptable but a little quantitatively different which is not surprising however due to the simplifications in the numerical model, particularly the simplified heat flux distribution on the inner surface of the motor frame. This test confirms the validity of the proposed simplified model at least for an investigation of the heat-dissipation power of a motor frame.

For a better performance, the temperature inside the motor must be maintained sufficiently low. As mentioned above, a temperature below 130°C is desired. Herein we examine the temperature on the inner surface of the frame and show it in Figure 8 in which θ=0° corresponds to the direction of six o'clock. Unacceptably high temperatures are observed in the regions attached with cooling ducts; the maximum temperature is found to be 140°C and is associated with the upper cooling duct which has a larger cross sectional area than the lower one. It seems the poor thermal conductivity of air in the cooling ducts causes huge thermal resistance and blocks heat transfer to the outer surface of the frame and the fins on it. The other region of poor heat dissipation is the near-floor region (small θ region). It is probably because, for the industrial TEFC motor under investigation, fins in the near-floor region are not shrouded by the wind shield and their heights are shorter due to the existence of the floor. A new frame that fixes the above two hot regions therefore becomes the target of this study.

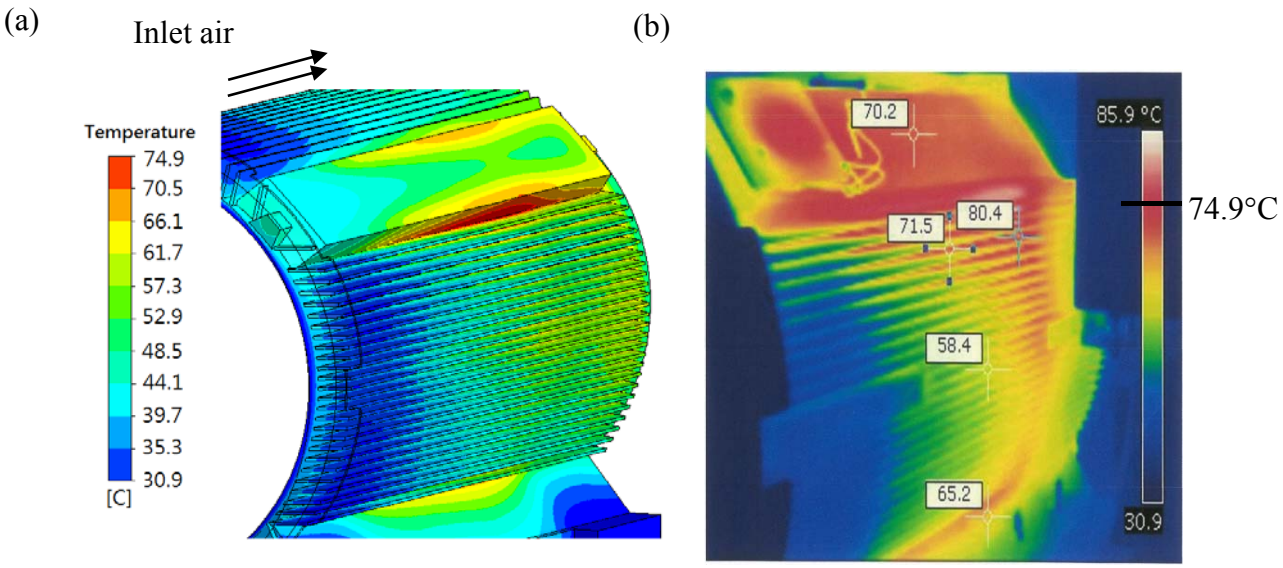

Figure 7. A comparison of the temperature distribution: (a) simulation, (b) experiment.

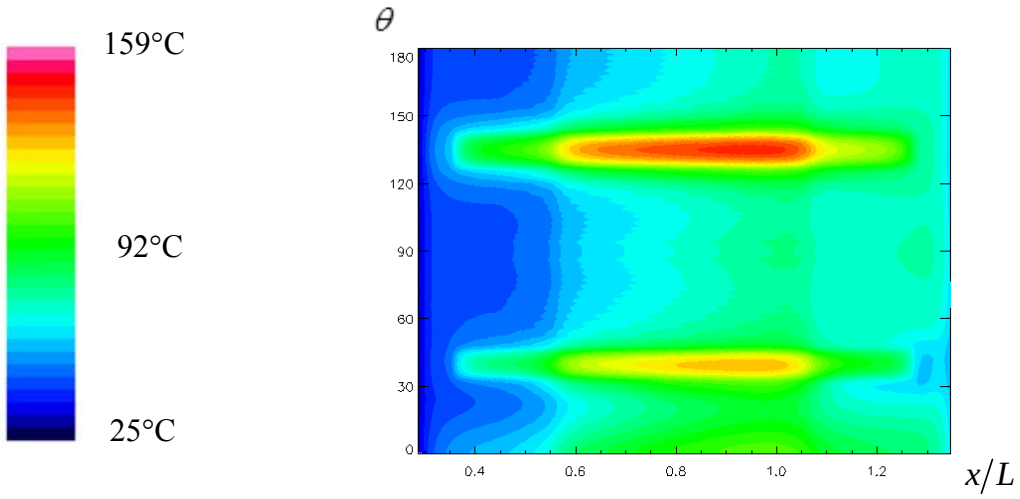

Figure 8. The simulated temperature contour on the inner surface of the motor frame. The total heat dissipation rate is 29kW.

3. New frame designs

In this section, the motor frame will be properly modified in order to diminish heat dissipation deficiencies associated with the original design. The design goals are a frame temperature below 130°C and a temperature difference in the azimuthal direction below 10°C. The design goals are associated with the certified insulation class B for motors [1].

3.1. The concept design

We know now that the existence of the cooling ducts causes hot spots. The cooling ducts are unavoidable however if a circulation flow is wanted inside the motor. To provide airways without causing serious hot spots, we propose to divide the cooling ducts to many more parts and distribute them as uniformly as possible over the motor frame as shown in Figure 9. The air blocks heat transfer still but the walls between neighboring ducts can help conducting heat like inner fins. For consistence, the total cross sectional area of these small cooling ducts is made as the same as that of the original design.

Several attempts are made to further improve the design. First of all, the cooling ducts are distributed from the 12 o'clock position to about the location of the stand; in other words, no cooling duct is embedded in the near-floor region because of the observed poor heat dissipation there in the original design. Besides, the thickness of the frame decreases gradually from the stand to the 6 o'clock position, hopefully to enhance thermal conduction toward the stands which are also made of cast iron and has a large contact area with ambient air. Furthermore, a flat plate is added between the two stands of the motor. It is connected to the wind shield and extended to the downstream end of the motor; it covers the flat-plate fins there so that air is trapped and an improved heat dissipation for the bottom of the motor can thus be expected.

The fin spacing of the outer fins must be optimized. Herein we adopt the model proposed by Knight et al. [29] but employ the empirical equations (2)–(5) for the evaluation of the friction factor and Nusselt number in order to take the turbulent effect and the roughness effect into consideration. The optimum spacing is determined based on a given fin thickness and height, the perimeter of the frame, and a range of pumping power. A same fin spacing is employed for the inner fins for direct thermal conduction from the inner surface to the outer surface of the frame [3]. There are of course several disparities between the model of Knight et al. [29] and the present application. In the model of Knight et al. [29], the fin arrays are fully shrouded and the region to be cooled is flat. In contrast, in the application of the TEFC motor frame, the outer fins are not shrouded so that the air flow rate decreases with increasing downstream distance. Therefore, from this viewpoint, the optimum fin spacing may be underestimated. On the other hand, because the motor frame is curved and we regard the so-predicted optimum spacing as the distance between fin bases, the actual cross sectional area between two neighboring fins is larger than the assumed one in the model. A higher air flow rate is consequently resulted and the model, from this concern, overestimates the optimum fin spacing. Because all these effects are too difficult to analyze and they cancel each other out to certain extent, we simply ignore them in the present study.

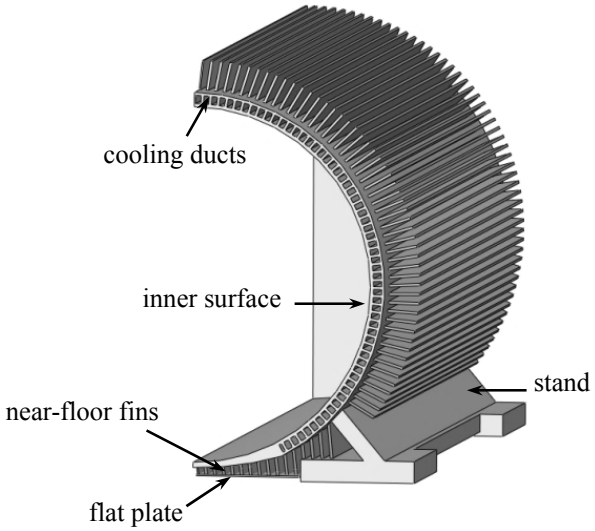

Figure 9. Concept design of the new motor frame.

3.2. Frame F1

Based on the concept mentioned in the previous subsection, we design the first frame, frame F1, which has a structure similar to that shown in Figure 9 except the upstream part of the frame. As we have noticed that the frame temperature is lower there due to smaller heat flux and stronger convection, the number of the inner fins may be reduced not only for the purpose of temperature uniformity but also for the sake of reducing the flow resistance. We thus decide to remove every other inner fin in the upstream part; that is, one upstream duct is split into two equal ones at the beginning of the midstream part. Figure 10 shows the upstream as well as the downstream cross sections and one whole cooling duct for illumination. Note that the so-called upstream, midstream, and the downstream regions are defined accorded with the heat flux boundary conditions shown in Figure 3, namely $x \in [x_0, x_0+L/4]$, $[x_0+L/4, x_0+3L/4]$, and $[x_0+3L/4, x_0+L]$ respectively, where x_0 is the location of the leading edges of the outer fins.

The simulation conditions are all the same as the original motor simulated in the last section. Same rules are employed for the grid generation as well and a total of 1012 million grid points is resulted. The temperature distribution on the inner surface of the frame F1 is compared with that of the original frame in Figure 11, in which the vertical dash lines indicate the boundaries between the upstream and midstream regions and between the midstream and the downstream regions. The new frame obviously has a much more uniform temperature distribution. The maximum temperature calculated is 75°C, much lower than the allowable one (130°C). By taking the difference between the maximum and minimum temperatures along the azimuthal direction, we find the temperature difference (ΔT) against the downstream distance in Figure 12. The criterion $\Delta T<10$°C is satisfied in most of the midstream and downstream regions. The large temperature difference in the upstream region is due to the strong heat dissipation in the near-floor region (because of shrouded fins and low air temperature). One may call it “cold spot” in contrast to “hot spot.” It makes no harm from

the practical viewpoint nonetheless because major components of the motor are located in the midstream region and the temperature is sufficiently low. The excessive temperature difference near the very end of the motor as observed in Figure 12 on the other hand is not serious and still tolerable. In remark, this new frame works successfully.

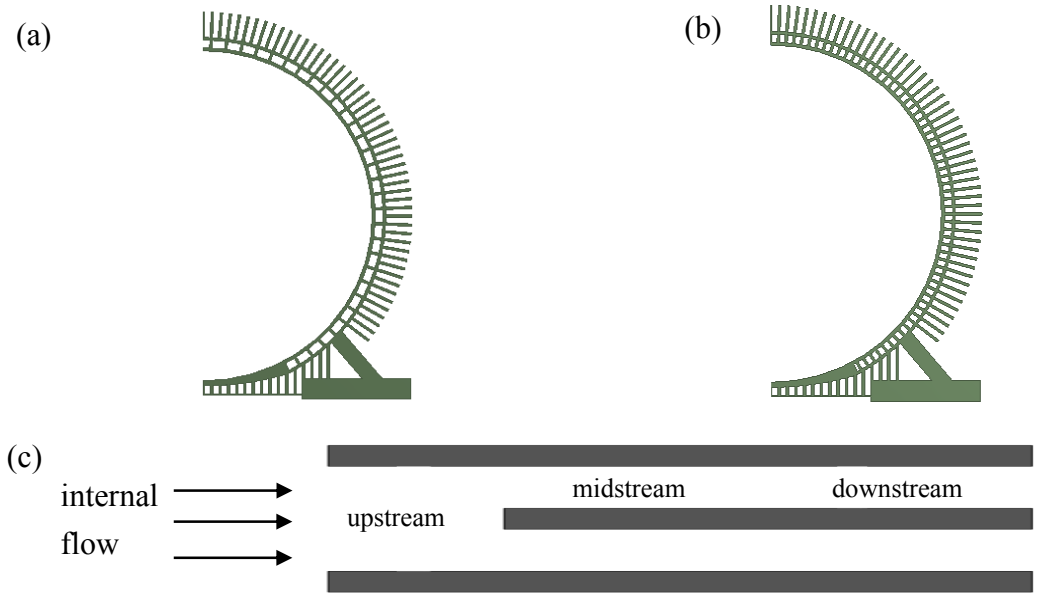

Figure 10. (a) Upstream, (b) midstream and downstream cross sections of frame F1; (c) an illustration of one cooling duct.

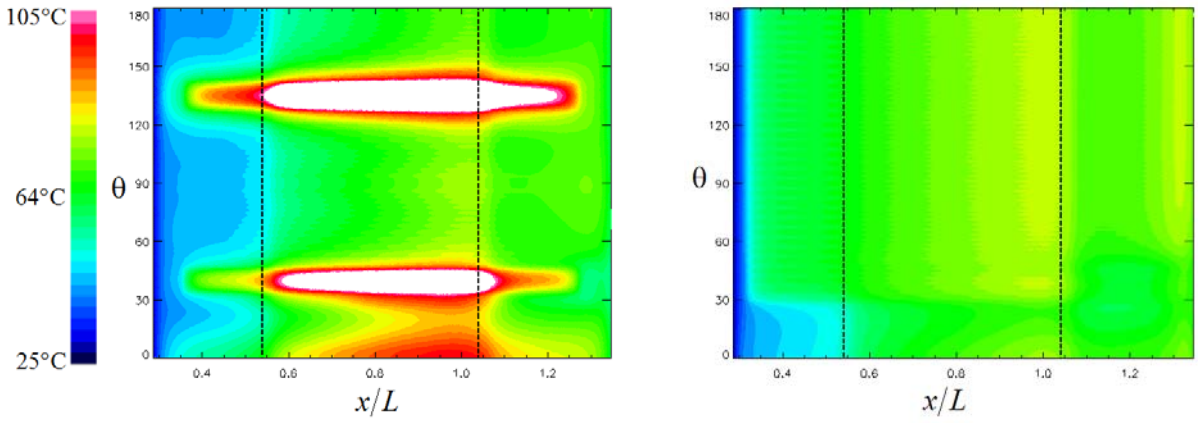

Figure 11. Temperature distributions over the inner surface of (a) the original frame and (b) Frame F1. The maximum temperatures are 140°C and 75°C respectively; the region having a temperature above 105°C is colored by white.

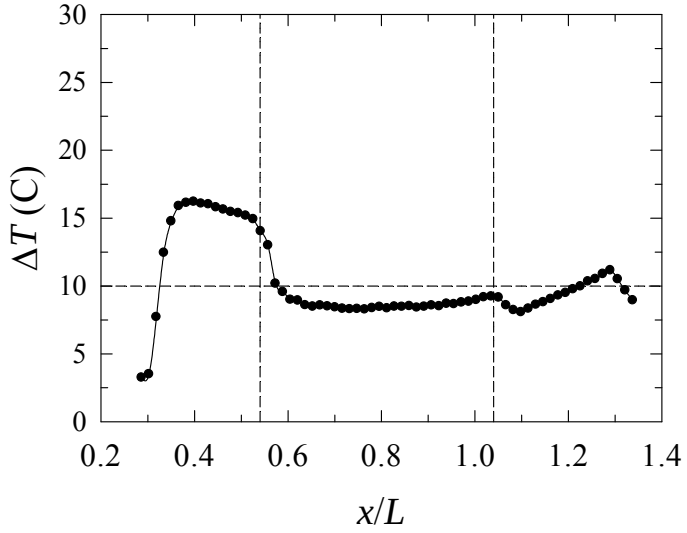

Figure 12. The maximum azimuthal temperature difference (ΔT) of the frame F1 against the downstream distance (x/L).

3.3. Frames F2 and F3

In spite of being successful, the frame F1 has small cooling ducts which may result in large flow resistance and difficulty in manufacture. Therefore we choose the second frame to have a similar structure as the frame F1 but retain only half inner fins as shown in Figure 13; the weight of the frame is also reduced. Figure 14 shows the simulation results. The maximum temperature is increased to 90°C, still lower than the maximum allowable one. The temperature uniformity is obviously not acceptable. The heat dissipation power is relatively too strong in the near-floor region now. Such a phenomenon was observed only in the upstream region of the frame F1. This problem can be easily fixed by reducing the outer fins in the near-floor region.

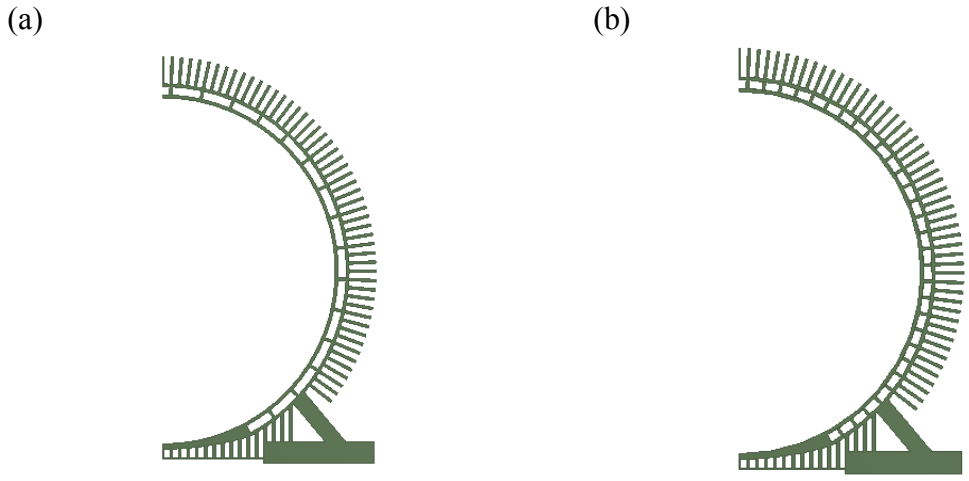

Figure 13. (a) Upstream, (b) midstream and downstream cross sections of the frame F2.

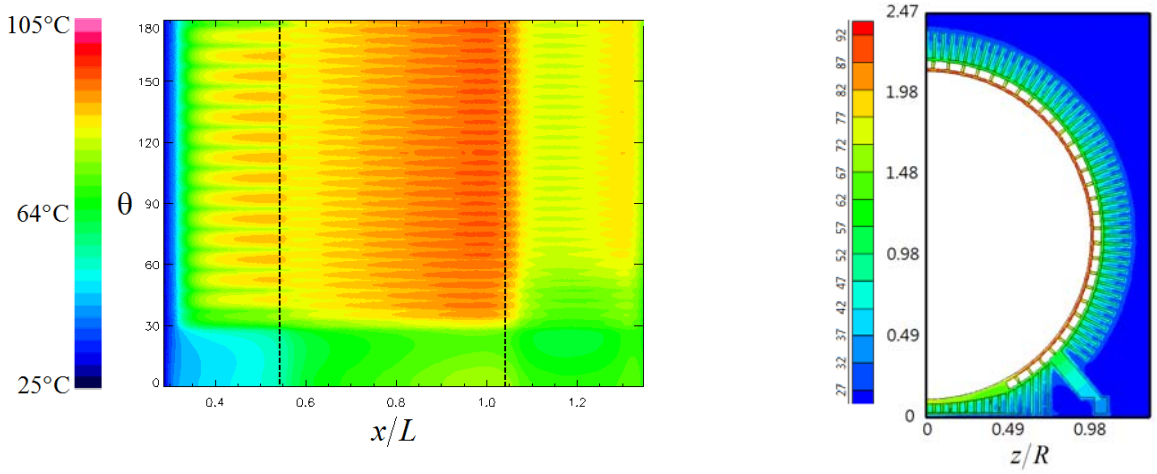

Figure 14. The temperature distributions over the inner surface of the frame F2 and on the cross section in the midstream region (x/L=0.96).

To avoid both hot spots and cold spots, the outer fins in the near-floor region must be carefully adjusted. Through a series of tests, we end up with a modified design, frame F3, as shown in Figure 15. One notices that the number of the near-floor fins are reduced from 16 in F1 and F2 to 9 in F3. Besides, the lengths of some fins are carefully adjusted according to the local situations. The upstream parts of 3 outer fins are removed because of small heat flux and cold air temperature there. The downstream part of one of them is also removed because of the observed green region above 30° in the downstream region from Figure 14.

The temperature distribution over the inner surface of the frame F3 is shown in Figure 16. The maximum temperature is 94°C, only slightly larger than that associated with F2. The temperature difference is below 10°C almost everywhere. We remark that frame F3 is also a successful design.

At the end, we show the temperature distributions along the azimuthal direction at several downstream distances of frames F1 and F3 in Figure 17. The vertical dash line indicates the starting position of the cooling ducts; to its left is the so-called near-floor region. The length adjustment of the outer fins in the frame F3 successfully increases the frame temperature in the near-floor region. The dips appearing in the distributions correspond to the locations of inner fins; peaks are results of the blockage of heat transfer caused by the air in the cooling ducts. The temperature difference is mainly caused by the cold near-floor region in frame F1 but by the dips and peaks in frame F3, implying a further reduction of the inner fins is not encouraged.

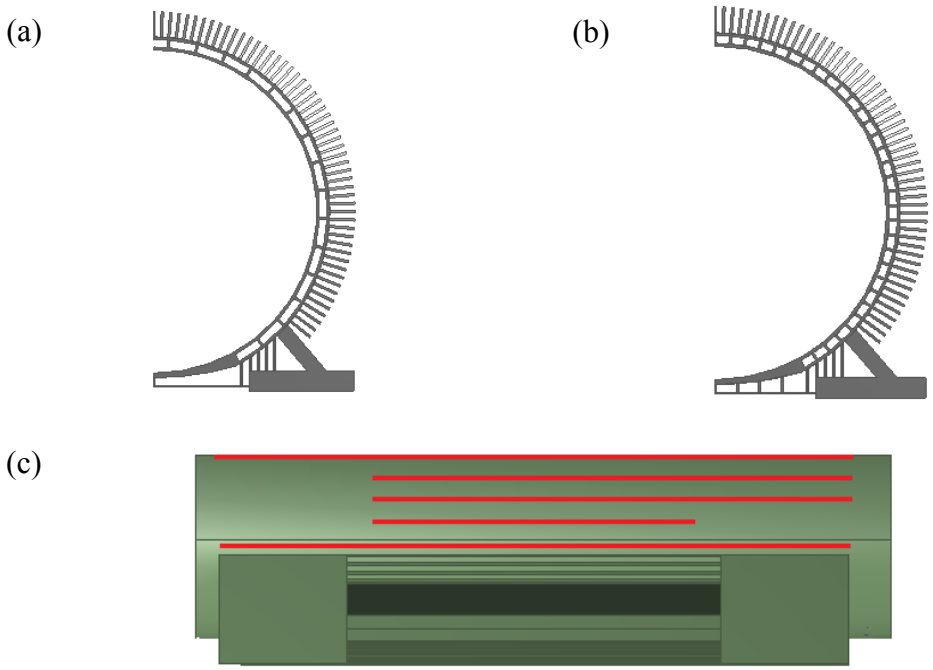

Figure 15. (a) The upstream, (b) midstream and downstream cross sections, and (c) a bottom view of the frame F3 in which 5 outer fins are shown in red (these outer fins are still shrouded by a flat-plate which is not shown in the figure).

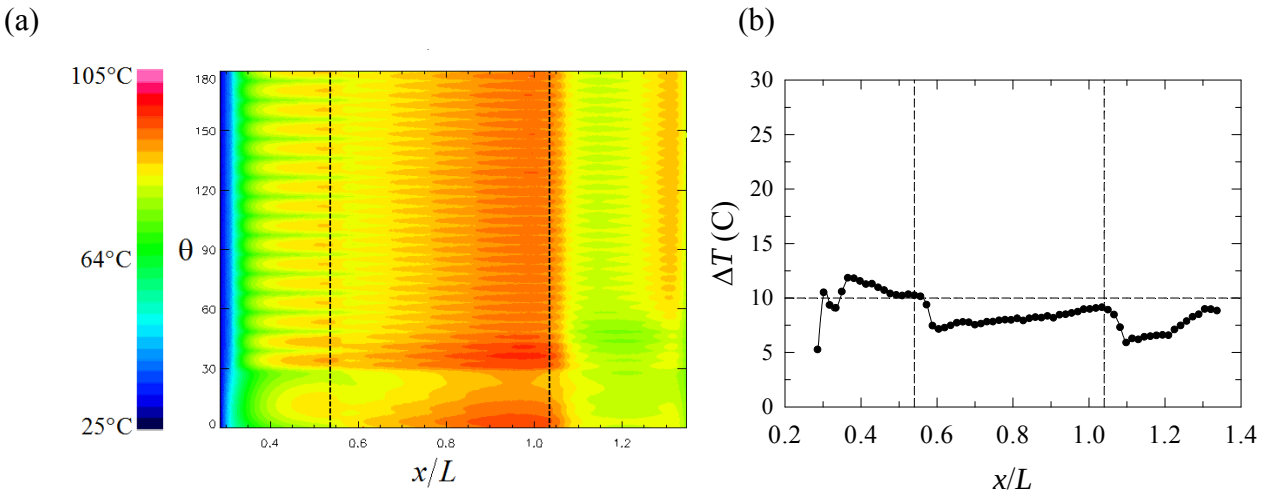

Figure 16. (a) The temperature distributions over the inner surface of the frame F3 and (b) the temperature difference against the downstream distance x/L.

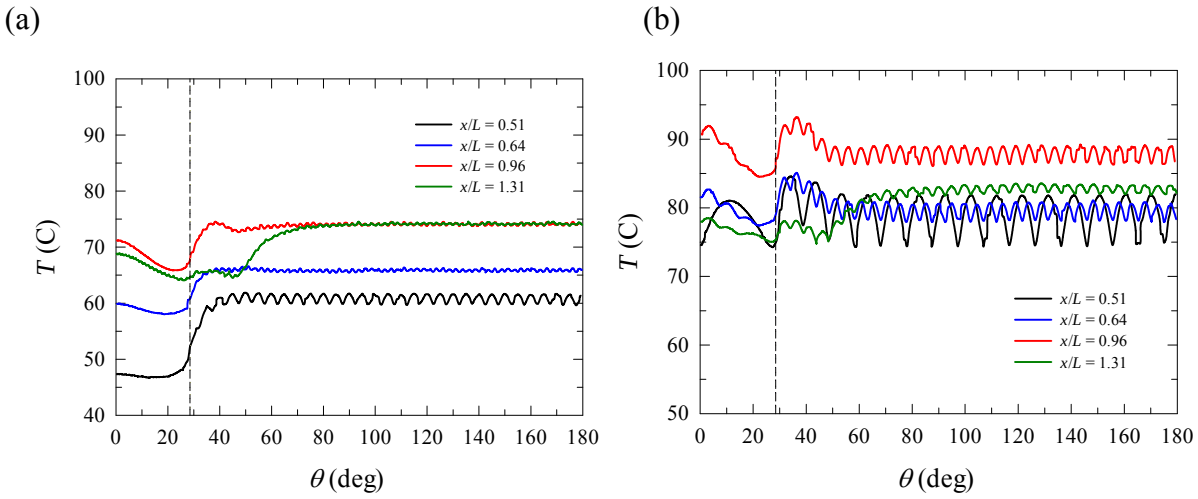

Figure 17. The temperature distributions along the azimuthal direction at several downstream distances of frames F1 (a) and F3 (b).

3.4. Flow resistance

It has been shown the new designs, frame F1 and frame F3, have a better thermal performance than the original one. The flow resistance of the cooling ducts however must increase and consequently so is the power consumption. In this subsection, we attempt to evaluate the involved flow resistances in the following way. Firstly we calculate the hydraulic diameters of the cross sections in the upstream and downstream sections. Equation (5) is next employed to evaluate the friction factors which in turn give the pressure drops across a distance $L/4$ and $3L/4$ respectively. The flow resistances defined as the ratio of the pressure drop to the air volume flow rate can then be obtained, denoted as R_u and R_d. The total flow resistance of a whole cooling duct (R_1) may be estimated as the result of connecting two R_d's in parallel first and one R_u in series next, as suggested by Figure 10(c). Finally the effective flow resistance of all the cooling ducts is R_1/N, where N is the number of cooling ducts.

The calculations reveal that the ratios of the flow resistances of frames F1 and F3 to that of the original design are 9.4 and 2.1 respectively. Notice the power consumption associated with the cooling ducts is only about 20W for frame F1 which is much less than the pumping power required for driving the internal flow through the core of the motor, not to mention the iron loss and the copper loss (on the order of kW). Therefore, we think there is no need to worry about the increased flow resistances and the pumping powers of frames F1 and F3.

4. Conclusions

A useful numerical model was proposed for investigating the heat dissipation capability of the frame of an industrial totally-enclosed-fan-cooled (TEFC) motor. The model is so simplified that the electromagnetic analysis can be avoided. In use of this model, two new motor frames were

successfully designed; the certified insulation class B for motors is satisfied. Several points are made based on the research results.

(1) The cooling ducts embedded within the motor frame block heat transfer unfortunately due to the poor thermal conductivity of air. Distributing them as uniform as possible along the azimuthal direction and using inner fins are suggested if these cooling ducts are necessary.

(2) The floor limits the height of the outer fins in the bottom part of the frame. To enhance heat dissipation there, it is better to have a cover that fully shrouds those outer fins. The lengths of these fins however must be properly adjusted to prevent from the occurrence of cold spots.

(3) The model proposed by Knight et al. [29] is useful for determining the optimum spacing of fins on the motor frame. Surely so are other similar models.

Acknowledgement

This work was supported by the TECO Electric & Machinery Co., Ltd., Taiwan.

Nomenclature

A_c	cross-section area of cooling duct
D_h	hydraulic diameter
f	friction coefficient
h	convection heat transfer coefficient
k_s	surface roughness of the motor
L	fin length
Nu	Nusselt number
P_{ch}	perimeter of cooling duct
Pr	Prandtl number
q	heat flux
R	internal radius of the motor frame
Re_D	Reynolds number based on hydraulic diameter
Re_t	Reynolds number based on fin thickness
R_F	flow resistance of a full cooling duct
$R_{F,d}$	flow resistance of the downstream small flow channel
$R_{F,u}$	flow resistance of the upstream large flow channel
T_{duct}	air tempature inside the cooling duct
U_{in}	inlet air velocity
x	streamwise coordinate
ΔT	maximum azimuthal temperature difference
θ	azimuthal coordinate
λ	air thermal conductivity
ν	kinematic viscosity

REFERENCES

[1] https://en.wikipedia.org/wiki/Insulation_system.

[2] R. N. Telore, M. P. Tunuguntla, and M. Doctor, Motor Cooling Arrangement, US patent 2008/0231126 A1, 2008.

[3] R. D. Lordo and W. E. Rudisch, Motor Frame and Motor with Increased Cooling Capacity, US patent 4,839,547, 1989.

[4] E. Hashish, Induction Motor Auxiliary Cooling System, US patent 2014/0021812 A1, 2014.

[5] S. T. Evon and W. E. Martin, Enhanced Electrical Machine Cooling, US patent 2006/0284511 A1, 2006.

[6] R. T. Dawsey, C. C. Stancu, E. R. Ostrom, and Y. Doo, Apparatus for Cooling Stator Lamination Stacks of Electrical Machines, US 2008/0100159 A1, 2008.

[7] K. Kinoshita, Cooling device of motor, US patent 7,615,897 B2, 2009.

[8] K. Kinoshita, Motor cooling device, EP 1 729 402A1, 2005.

[9] R. Beatty, B.A. Trago, G.W. Brown, I. Hovey, and R. Bishop, Cooling of electric motor with coolant pipe and conduction plates or cups, US patent 8,405,262 B1, 2013.

[10] M.C. Smith, A. Ritchie, V. Caron, D.A. Kramer, Method for forming a cooling jacket for an electric motor, US patent 8,161,643 B2, 2012.

[11] M. Fiebig, Embedded Vortices in Internal Flow: Heat Transfer and Pressure Loss Enhancement, *Int. J. Heat Fluid Flow*, vol. 16, pp. 376–388, 1995.

[12] O. Leon, G. Mey, E. Dick, and J. Vierendeels, Comparison Between the Standard and Staggered Layout for Cooling Fins in Forced Convection Cooling, *J. Electron Packaging*, vol. 125, pp. 442–446, 2003.

[13] Y. J. Lee, P. S. Lee, and S. K. Chou, Numerical Study of Fluid Flow and Heat Transfer in the Enhanced Microchannel with Oblique Fins, *J. Heat Transfer*, vol. 135, issue 4, 041901, 2013.

[14] M. R. Shaeri, M. Yaghoubi, and K. Jafarpur, Heat Transfer Analysis of Lateral Perforated Fin Heat Sinks, *Appl. Energy*, vol. 86, pp. 2019–2029, 2009.

[15] M. F. Ismail, M. N. Hasan, and S. C. Saha, Numerical Study of Turbulent Fluid Flow and Heat Transfer in Lateral Perforated Extended Surfaces, *Energy*, vol. 64, pp. 632–639, 2014.

[16] Y. Islamoglu and C. Parmaksizoglu, The Effect of Channel Height on The Enhanced Heat Transfer Characteristics in a Corrugated Heat Exchanger Channel, *Appl. Therm. Eng.*, vol. 23, pp. 979–987, 2003.

[17] P. Naphon, Heat Transfer Characteristics and Pressure Drop in Channel with V Corrugated Upper and Lower Plates, *Energy Convers. Manage.*, vol. 48, pp. 1516–1524, 2007.

[18] M. Morega and A. Bejan, Plate Fins with Variable Thickness and Height for Air-Cooled Electronic Modules, *Int. J. Heat Mass Transfer*, vol. 37, suppl. 1, pp. 433–445, 1994.

[19] D. K. Kim, J. Jung, and S. J. Kim, Thermal Optimization of Plate-Fin Heat Sinks with Variable Fin Thickness, *Int. J. Heat Mass Transfer*, vol. 53, pp. 5988–5995, 2010.

[20] M. Dogan and M. Sivrioglu, Experimental and Numerical Investigation of Clearance Gap

Effects on Laminar Mixed Convection Heat Transfer From Fin Array in A Horizontal Channel – A Conjugate Analysis, *Appl. Therm. Eng.*, vol. 40, pp. 102–113, 2012.

[21] D. Soodphakdee, M. Behnia, and D.W. Copeland, A comparison of fin geometries for heatsinks in laminar forced convection: Part I-round, elliptical, and plate fins in staggered and in-line configurations, Inter. J. Microcircuits and Electronic Packaging 24, 68-76, 2001.

[22] D. Soodphakdee, M. Behnia, and D.W. Copeland, A comparison of fin geometries for heatsinks in laminar forced convection: Part II-optimization of staggered plate fin heatsink, Inter. J. Microcircuits and Electronic Packaging 24, 77-83, 2001.

[23] A.B. Ganorkar and V.M. Kriplani, Review of heat transfer enhancement in different types of extended surfaces, Inter. J. Engr. Sci. & Tech. 3, 3304-3313, 2011.

[24] A. Bar-Cohen and W.M. Rohsenow, Thermally Optimum Spacing of Vertical, Natural Convection Cooled, Parallel Plates, *J. Heat Transfer*, vol. 106, pp. 116–123, 1984.

[25] S.W. Churchill and R. Usagi, A General Expression for the Correlation of Rates of Transfer and Other Phenomena, *AIChE J.*, vol. 18, no. 6, pp. 1121–1128, 1972.

[26] A. Bejan and E. Sciubba, The Optimal Spacing of Parallel Plates Cooled by Forced Convection, *Int. J. Heat Mass Transfer*, vol. 35, no. 12, pp. 3259–3264, 1992.

[27] A. Bejan and A. M. Morega, The Optimal Spacing of a Stack of Plates Cooled by Turbulent Forced Convection, *Int. J. Heat Mass Transfer*, vol. 37, no. 6, pp. 1045–1048, 1994.

[28] P. Canhoto and A. H. Reis, Optimization of Forced Convection Heat Sinks with Pumping Power Requirements, *Int. J. Heat Mass Transfer*, vol. 54, issues 7–8, pp. 1441–1447, 2011.

[29] R. W. Knight, D. J. Hall, J. S. Goodling, and R. C. Jaeger, Heat Sink Optimization with Application to Microchannels, *IEEE Trans. Comp., Hybrids, Manufact. Technol.*, vol. 15, pp. 832–842, 1992.

[30] Hossain R., Culham J.R., and Yovanovich M.M., Influence of bypass on flow through plate fin heat sinks, 23rd IEEE SEMI-THERM Symposium, 2007.

[31] C. J. Shih and G. C. Liu, Optimal Design Methodology of Plate-Fin Heat Sinks for Electronic Cooling Using Entropy Generation Strategy, *IEEE T. Compon. Pack. T.*, vol. 27, no. 3, pp. 551-559, 2004.

[32] D. J. Zigrang and N. D. Sylvester, Explicit Approximations to the Solution of Colebrook Friction Factor Equation, *AIChE J.*, vol. 28, pp. 514–515, 1982.

[33] A. T. Wassel and A. F. Mills, Calculation of Variable Property Turbulent Friction and Heat Transfer in Rough Pipes, *J. Heat Transfer*, vol. 101, pp. 469–474, 1979.

[34] E. Velayati and M. Yaghoubi, Numerical Study of Convection Heat Transfer from An Array of Parallel Bluff Plates, *Int. J. Heat Fluid Flow*, vol. 26, pp. 80–91, 2005.